AMPK negatively regulates tensin-dependent integrin activity

Maria Georgiadou,[1]* Johanna Lilja,[1]* Guillaume Jacquemet,[1] Camilo Guzmán,[1] Maria Rafaeva,[1] Charlotte Alibert,[3,4] Yan Yan,[5] Pranshu Sahgal,[1] Martina Lerche,[1] Jean-Baptiste Manneville,[3,4] Tomi P. Mäkelä,[5] and Johanna Ivaska[1,2]

[1]Turku Centre for Biotechnology and [2]Department of Biochemistry, University of Turku, FI-20520 Turku, Finland
[3]Institut Curie, Paris Sciences et Lettres Research University and [4]Sorbonne Universités, Université Pierre et Marie Curie (UPMC) Université Paris 06, Centre National de la Recherche Scientifique, UMR144, F-75005 Paris, France
[5]Research Programs Unit, Faculty of Medicine, University of Helsinki, FI-00014 Helsinki, Finland

Tight regulation of integrin activity is paramount for dynamic cellular functions such as cell matrix adhesion and mechanotransduction. Integrin activation is achieved through intracellular interactions at the integrin cytoplasmic tails and through integrin–ligand binding. In this study, we identify the metabolic sensor AMP-activated protein kinase (AMPK) as a β1-integrin inhibitor in fibroblasts. Loss of AMPK promotes β1-integrin activity, the formation of centrally located active β1-integrin– and tensin-rich mature fibrillar adhesions, and cell spreading. Moreover, in the absence of AMPK, cells generate more mechanical stress and increase fibronectin fibrillogenesis. Mechanistically, we show that AMPK negatively regulates the expression of the integrin-binding proteins tensin1 and tensin3. Transient expression of tensins increases β1-integrin activity, whereas tensin silencing reduces integrin activity in fibroblasts lacking AMPK. Accordingly, tensin silencing in AMPK-depleted fibroblasts impedes enhanced cell spreading, traction stress, and fibronectin fiber formation. Collectively, we show that the loss of AMPK up-regulates tensins, which bind β1-integrins, supporting their activity and promoting fibrillar adhesion formation and integrin-dependent processes.

Introduction

AMP-activated protein kinase (AMPK) is a serine/threonine kinase and a prominent metabolic sensor in cells. At the cellular level, energy stress leads to the activation of AMPK, which inhibits energy-consuming anabolic pathways and triggers energy-promoting catabolic pathways (Hardie et al., 2012). Because of the critical role of AMPK in metabolic regulation, this kinase has become an attractive therapeutic target for the treatment of obesity, diabetes, and cancer (Hardie, 2013). Apart from its well-described role in maintaining cellular energy homeostasis, AMPK regulates several other physiological processes, including cell growth, autophagy, cell polarity, development, mitosis, and transcription (Zhang et al., 2006; Lee et al., 2007; Nakano et al., 2010; Banko et al., 2011; Mihaylova and Shaw, 2011; Schaffer et al., 2015). In a screen performed recently in human cancer cell lines, many newly identified AMPK substrates consisted of proteins involved in cell motility, adhesion, and invasion (Schaffer et al., 2015). Nevertheless, the role of AMPK in cell adhesion and mechanotransduction remains largely underexplored.

Integrins are transmembrane receptors that mediate cell–matrix interactions, with key functions in cell adhesion, migration, and mechanotransduction. Integrins are heterodimers, consisting of an α and a β subunit, and exist at the plasma membrane in either the bent (inactive) conformation or the extended (active) conformation (Hynes, 2002). Integrin binding to ECM ligands promotes conformational changes within the receptor that favor integrin activation in a process called outside-in signaling. Alternatively, several proteins bound to the intracellular part of integrins regulate receptor conformation and thus activity via so-called inside-out activation (Kim et al., 2011). Talins and kindlins are both well-described integrin activators, which bind the cytoplasmic tail of β-integrins (Calderwood et al., 2013). Conversely, other proteins, such as SHARPIN, DOK-1, ICAP1, and filamin, inhibit integrin activation by directly or indirectly disrupting the integrin–talin interaction (Bouvard et al., 2013). One family of proteins, known as tensins, bind integrins at a region overlapping with the talin-binding site (McCleverty et al., 2007), yet the role of this family in influencing integrin inside-out activation has not been investigated.

We found that the major metabolic sensor AMPK is an inhibitor of β1-integrin activity. Loss of AMPK promotes

*M. Georgiadou and J. Lilja contributed equally to this paper.

Correspondence to Johanna Ivaska: johanna.ivaska@utu.fi; or Maria Georgiadou: maria.georgiadou@utu.fi

Abbreviations used: ACC, acetyl-CoA carboxylase; AMPK, AMP-activated protein kinase; KO, knockout; MEF, mouse embryonic fibroblast; PTB, phosphotyrosine-binding; RTCA, real-time cell analysis; SLL, standard linear liquid; TFM, traction force microscopy; TIF, telomerase-immortalized fibroblast; TIRF, total internal reflection fluorescence; WT, wild type.

The Rockefeller University Press $30.00
J. Cell Biol. Vol. 216 No. 4 1107–1121
https://doi.org/10.1083/jcb.201609066

integrin activity and the formation of mature fibrillar adhesions with high levels of active α5β1-integrin and tensin. We further show that tensins can activate integrins and that AMPK inhibits β1-integrin activity by negatively regulating tensin levels. Congruently, AMPK-mediated inhibition of cell spreading, traction stress, and ECM assembly are tensin dependent.

Results

AMPK negatively regulates β1-integrin activity

AMPK is a heterotrimeric protein complex consisting of the catalytic α subunit and the regulatory β and γ subunits with at least two isoforms each (α1, α2; β1, β2; γ1, γ2, γ3; Hardie et al., 2012). Based on quantitative proteomic analyses, AMPK is a component of the fibronectin-induced integrin adhesome, as different subunits were identified in three independent mass spectrometry–based proteomics datasets (Schiller et al., 2013; Horton et al., 2015; Robertson et al., 2015). Moreover, AMPK is a putative β1-integrin inactivator. Indeed, in the kinome RNAi screen we performed previously (Rantala et al., 2011), two independent siRNAs against *PRKAA2* (AMPKα2) and one of two siRNAs targeting the AMPK regulatory β subunit *PRKAB2* (AMPKβ2) significantly increased β1-integrin activity. Interestingly, the regulatory γ subunit (AMPKγ2) is also associated with integrin activity, as it was identified as a putative integrin inhibitor in the druggable genomewide RNAi screen we performed in prostate cancer cells (VCap; Pellinen et al., 2012) and as a potential adhesome component associated with inactive β1-integrins (Byron et al., 2015).

To validate the role of AMPK in integrin activity suggested by these unbiased screens, we used immortalized mouse embryonic fibroblasts (MEFs) with wild-type (WT) AMPKα ($\alpha1^{+/-};\alpha2^{+/+}$) or with nullizygous AMPKα1 ($\alpha1^{-/-};\alpha2^{+/+}$ or α1-knockout [KO; α1KO]), AMPKα2 ($\alpha1^{+/-};\alpha2^{-/-}$ or α2KO), or both ($\alpha1^{-/-};\alpha2^{-/-}$ or KO), as described previously (Yan et al., 2015). We measured cell surface active integrins by flow cytometry (based on the binding of a recombinant integrin ligand fragment, fibronectin repeats 7–10 [FN7–10]) relative to total cell surface β1-integrin (Hughes et al., 2002; Tadokoro et al., 2003) and observed a modest increase in integrin activity upon the loss of one AMPKα isoform (α1KO or α2KO) and a significant increase upon the loss of both AMPKα isoforms (KO) compared with WT MEFs (Figs. 1 A and S1 A). Silencing of the remaining second isoform in the α1KO or α2KO (siα2 or siα1, respectively; Figs. 1 A and S1 A) significantly elevated integrin activity to the same extent as the loss of AMPKα in KO MEFs. Thus, both AMPKα isoforms suppress integrin activity. Consistently, loss of AMPKα in MEFs increased active β1-integrin levels as measured using the 9EG7 antibody recognizing the extended conformation of β1-integrin (Fig. S1 B; Byron et al., 2009; Askari et al., 2010). AMPKα also suppressed integrin activity in human cells. Silencing AMPKα1 alone with two independent siRNAs (Fig. S1 C) or both AMPKα1 and AMPKα2 isoforms (termed siAMPK; Fig. 1 B) in human telomerase-immortalized fibroblasts (TIFs) increased integrin activity compared with control-silenced TIFs. Moreover, treatment with the AMPK inhibitor dorsomorphin (also known as Compound C) promoted β1-integrin activity in TIFs (Fig. 1 C). Importantly, AMPK silencing significantly increased the level of and the adhesion area occupied by active β1-integrin compared with control-silenced cells as measured by high-resolution total internal reflection fluorescence (TIRF) microscopy (Figs. 1 D and S1 D). AMPK silencing was nearly as efficient in activating β1-integrins as exogenous stimulation with Mn^{2+} (Fig. S1 E). Collectively, AMPK inhibits β1-integrin activity in fibroblasts.

AMPK depletion promotes fibrillar adhesion formation

Given the striking effect of AMPK silencing on the distribution of active β1-integrin (Fig. 1 D), we assessed in more detail the localization of active β1-integrin in cells plated on fibronectin-coated crossbow-shaped micropatterns, enabling normalization for cell shape (Alanko et al., 2015). Representative images of individual cells (Fig. 2 A) and mean intensity heat maps of multiple cells addressing overall protein distribution (Chen et al., 2014b) revealed more active β1-integrin after AMPK deletion in centrally located adhesions in MEFs (Fig. 2, A and B) and in TIFs (Fig. S2 A).

In fibroblasts, integrins translocate centripetally from focal adhesions to mature, centrally located, elongated matrix contacts termed "fibrillar adhesions," which are enriched in active α5β1-integrin and tensin (Pankov et al., 2000; Zamir et al., 2000). To explore whether the ability of AMPK to suppress integrin activity is related to fibrillar adhesion formation, we assessed the distribution of the active (ligand bound) α5β1-integrin (SNAKA51 antibody; Clark et al., 2005) and tensin1 in spreading TIFs (because of antibody limitations, we were unable to study endogenous active mouse α5β1 and tensin in MEFs) using a high-resolution TIRF microscope. Active α5β1-integrin and tensin1 covered a larger cell area (Fig. 2, C and D), and active integrins showed a high degree of colocalization with tensin1 (Fig. 2, E and F) in AMPK-silenced TIFs compared with controls. In contrast, the β1-integrin activator talin1 covered a smaller area in AMPK-silenced TIFs compared with control-silenced cells (Fig. S2 B). Thus, loss of AMPK promotes β1-integrin activity in conjunction with an increased formation of fibrillar adhesions.

Loss of AMPK enhances cell adhesion and fibrillogenesis

Integrin activation and mature matrix adhesions are associated with increased cell adhesion and spreading (Geiger and Yamada, 2011; Theodosiou et al., 2016). Accordingly, cell spreading on fibronectin, mediated predominantly by α5β1- and αv-integrins, was markedly enhanced in AMPK KO MEFs compared with WT cells and in AMPK-silenced TIFs compared with control-silenced cells (Figs. 3 A and S3 A). There was no significant difference in the adhesion of AMPK WT and KO MEFs on vitronectin, the ECM ligand for αvβ3- and αvβ5-integrins (Fig. S3 B), suggesting that the loss of AMPK specifically affects the activity of β1-integrins (in this case α5β1-integrin). Integrin activation and fibrillar adhesions are also essential in ECM remodeling and fibronectin fibrillogenesis (Zamir et al., 2000; Gudzenko and Franz, 2015). Congruently with increased fibrillar adhesions in AMPK KO MEFs, we observed significantly longer fibronectin fibers in AMPK KO MEFs supplemented with exogenous fibronectin compared with WT cells (Fig. 3 B). Collectively, AMPK is a negative regulator of essential integrin activity–dependent functions such as cell spreading and matrix remodeling.

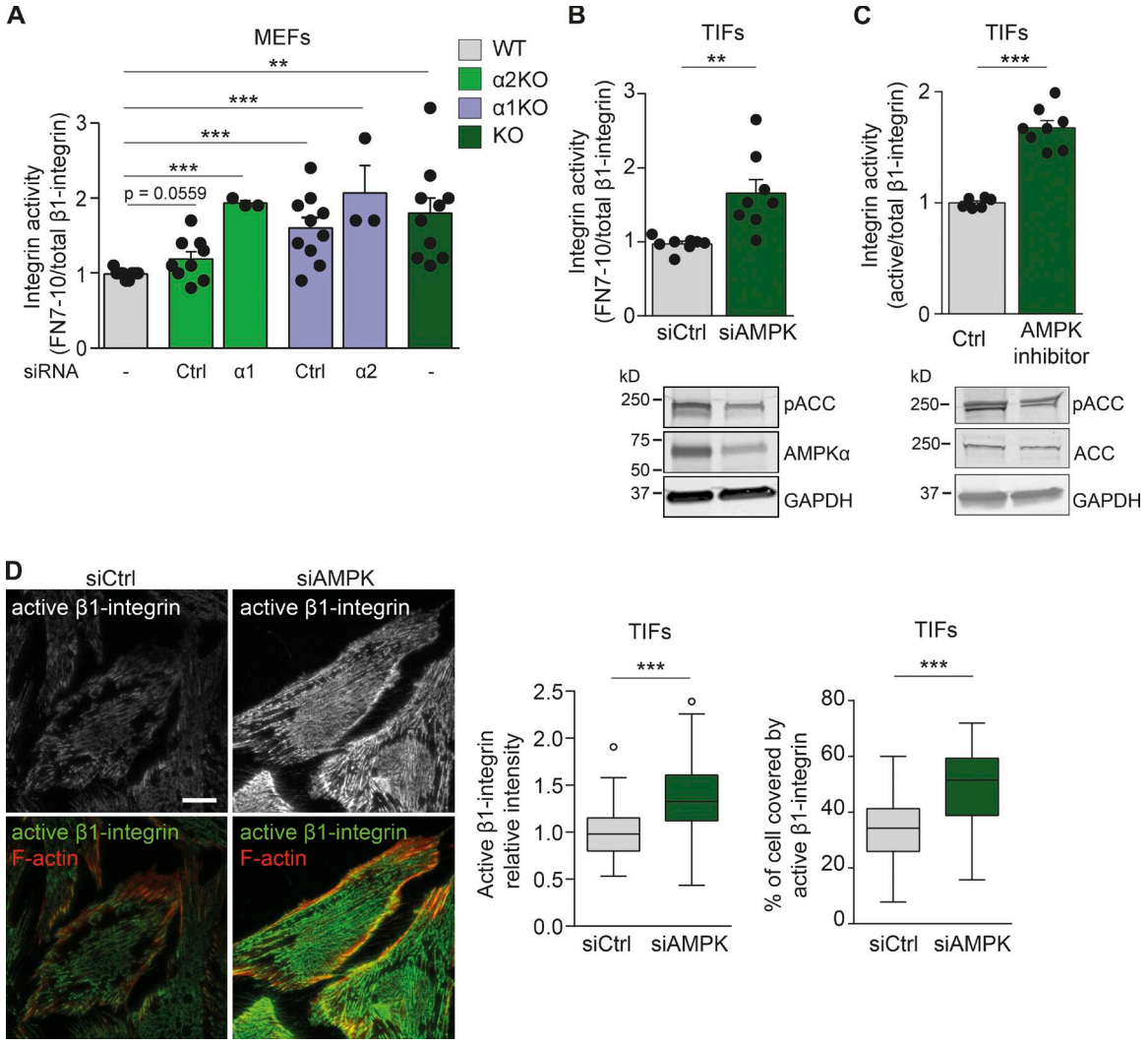

Figure 1. **AMPK negatively regulates β1-integrin activity.** (A) Quantification of flow cytometric assays of β1-integrin activity assessed as FN7–10 binding relative to total β1-integrin surface (MB1.2) levels in MEFs. Data and significance are expressed relative to WT AMPK MEFs and display means ± SEM. 10,000 cells were used per experiment. The number of independent experiments per condition (*n*) is represented with black dots. WT refers to MEFs expressing the catalytic AMPKα1 and AMPKα2 isoforms. α2KO and siCtrl refer to MEFs lacking the AMPKα2 catalytic subunit and silenced with control siRNA (P = 0.0559). α2KO and siα1 refer to MEFs lacking the AMPKα2 catalytic subunit and silenced for the remaining AMPKα1 subunit (***, P < 0.0001). α1KO and siCtrl refer to MEFs lacking the AMPKα1 catalytic subunit and silenced with control siRNA (***, P = 0.0009). α1KO and siα2 refer to MEFs lacking the AMPKα1 catalytic subunit and silenced for the remaining AMPKα2 subunit (***, P = 0.0002). KO refers to MEFs lacking both AMPKα catalytic isoforms (**, P = 0.0015). A two-tailed Student's *t* test was used to obtain p-values. (B) Quantification of flow cytometric assays of β1-integrin activity assessed as FN7–10 binding relative to total β1-integrin (P5D2) in TIFs silenced with control siRNA (siCtrl) or with siRNAs against AMPKα1 and AMPKα2 isoforms (siAMPK). Data are expressed relative to siCtrl and represent means ± SEM. 10,000 cells were used per experiment. **, P = 0.0025 (two-tailed Student's *t* test). Below are immunoblots assessing AMPKα expression and phosphorylation levels of the AMPK target ACC (pACC). GAPDH was used as a loading control. (C) Quantification of flow cytometric assays of β1-integrin activity assessed as FN7–10 binding relative to total β1-integrin (P5D2) in TIFs treated for 24 h with 10 µM dorsomorphin (AMPK inhibitor). Data are expressed relative to control and represent means ± SEM. 10,000 cells were used per experiment. ***, P < 0.0001 (two-tailed Student's *t* test). Below are immunoblots assessing the phosphorylation levels of pACC and total levels of ACC. GAPDH was used as a loading control. (D) Representative TIRF microscopy images of TIFs silenced for control (siCtrl) or AMPK (siAMPK), plated on fibronectin for 7 h, and stained for active β1-integrin (12G10) and F-actin (phalloidin). The level and coverage of active β1-integrin were determined and displayed as Tukey box plots. *n* > 120 cells from three biological repeats. ***, P < 0.0001 (two-tailed Student's *t* test). Bar, 20 µm.

Loss of AMPK enhances mechanotransduction and intracellular stiffness

Fibronectin fibrillogenesis is directed by traction forces (Lemmon et al., 2009), and integrins represent the main mechanotransducers of the cell (Schwarz and Gardel, 2012). Therefore, we sought to explore whether AMPK regulates the mechanical stress exerted by MEFs on fibronectin-coated polyacrylamide gels using traction force microscopy. Indeed, AMPK KO cells generated higher traction forces compared with WT cells (Fig. 3 C), in accordance with a previous study showing that β1-integrin activation promotes the generation of cellular traction forces (Lin et al., 2013).

The mechanical properties within the cell contribute to cell adhesion and traction stress generation, with β1-integrin being a major positive mediator of the intracellular mechanical state (Baker et al., 2009). We thus decided to assess the intracellular mechanical parameters of AMPK WT and KO MEFs using confocal microscopy and the recently developed intracellular micromanipulation technique, which measures

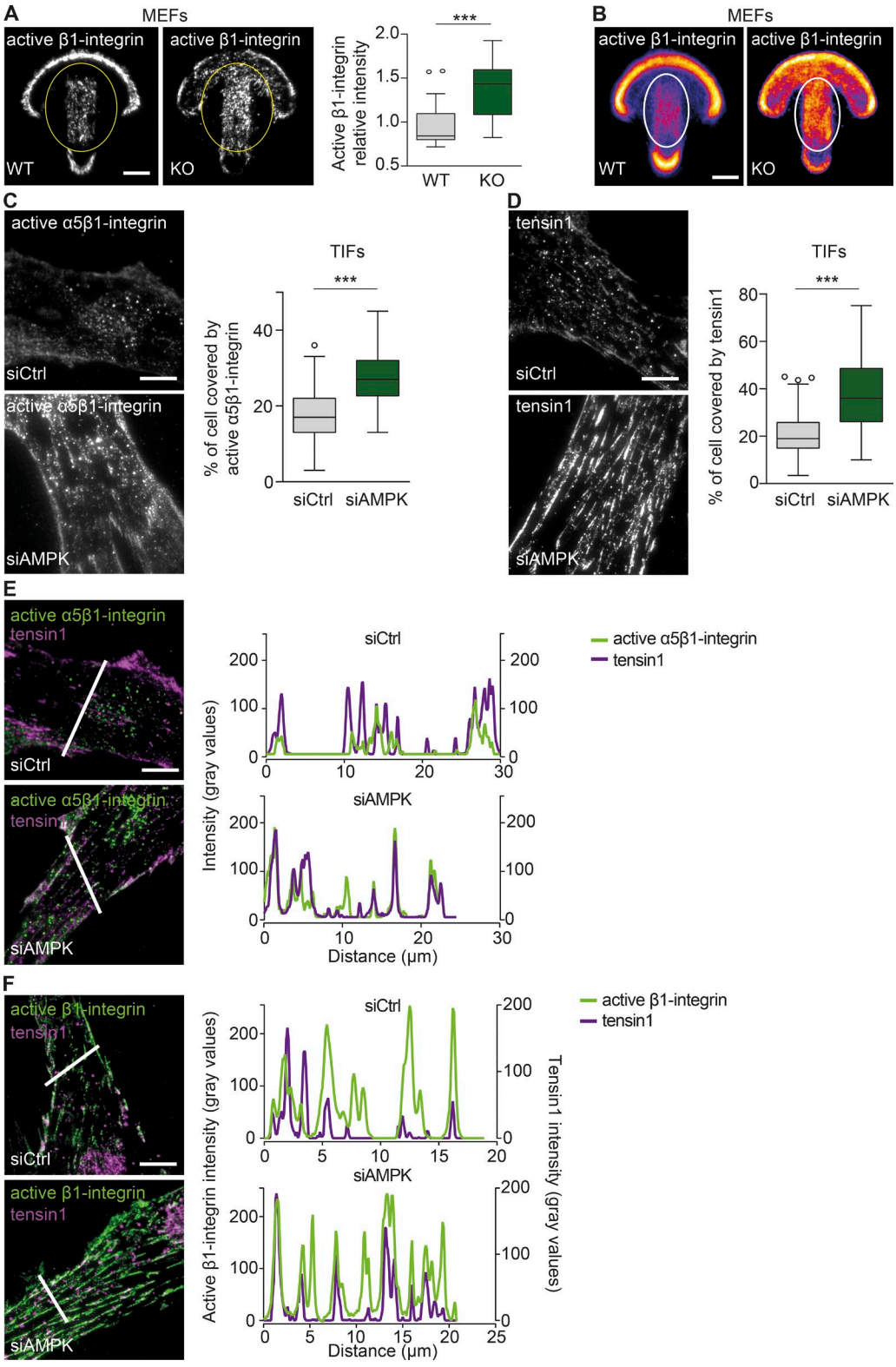

Figure 2. **AMPK depletion promotes fibrillar adhesion formation.** (A and B) Representative TIRF microscopy images (A) and mean intensity maps (B) of active β1-integrin immunofluorescence (9EG7) in AMPK WT and KO MEFs plated on fibronectin-coated crossbow-shaped micropatterns. The level of active β1-integrin (blue, low level; yellow, high level) within the yellow ovals was quantified (A) and displayed as Tukey box plots. $n > 25$ cells from two biological repeats. The mean active β1-integrin distribution is represented with a heat map (B), wherein yellow corresponds to regions within the cell containing the largest accumulation of active β1-integrin. The white ovals indicate the centrally located adhesions. $n = 20$ cells. (C and D) Representative TIRF microscopy images and quantification of active α5β1-integrin (SNAKA51; C) and tensin1 (D) distribution in siCtrl and siAMPK TIFs plated on fibronectin for 7 h. Data are displayed as Tukey box plots. $n > 70$ cells (C) and $n > 180$ cells (D) from three biological repeats. (A, C, and D) ***, $P < 0.0001$ (two-tailed Student's *t* test). (E and F) Representative TIRF microscopy images and plot profiles of siCtrl and siAMPK TIFs plated on fibronectin for 7 h and stained for either active α5β1-integrin (SNAKA51) and tensin1 (E) or for active β1-integrin (12G10) and tensin1 (F). Intensity profiles of the respective molecules were obtained across the white lines in each corresponding image. Bars, 10 μm.

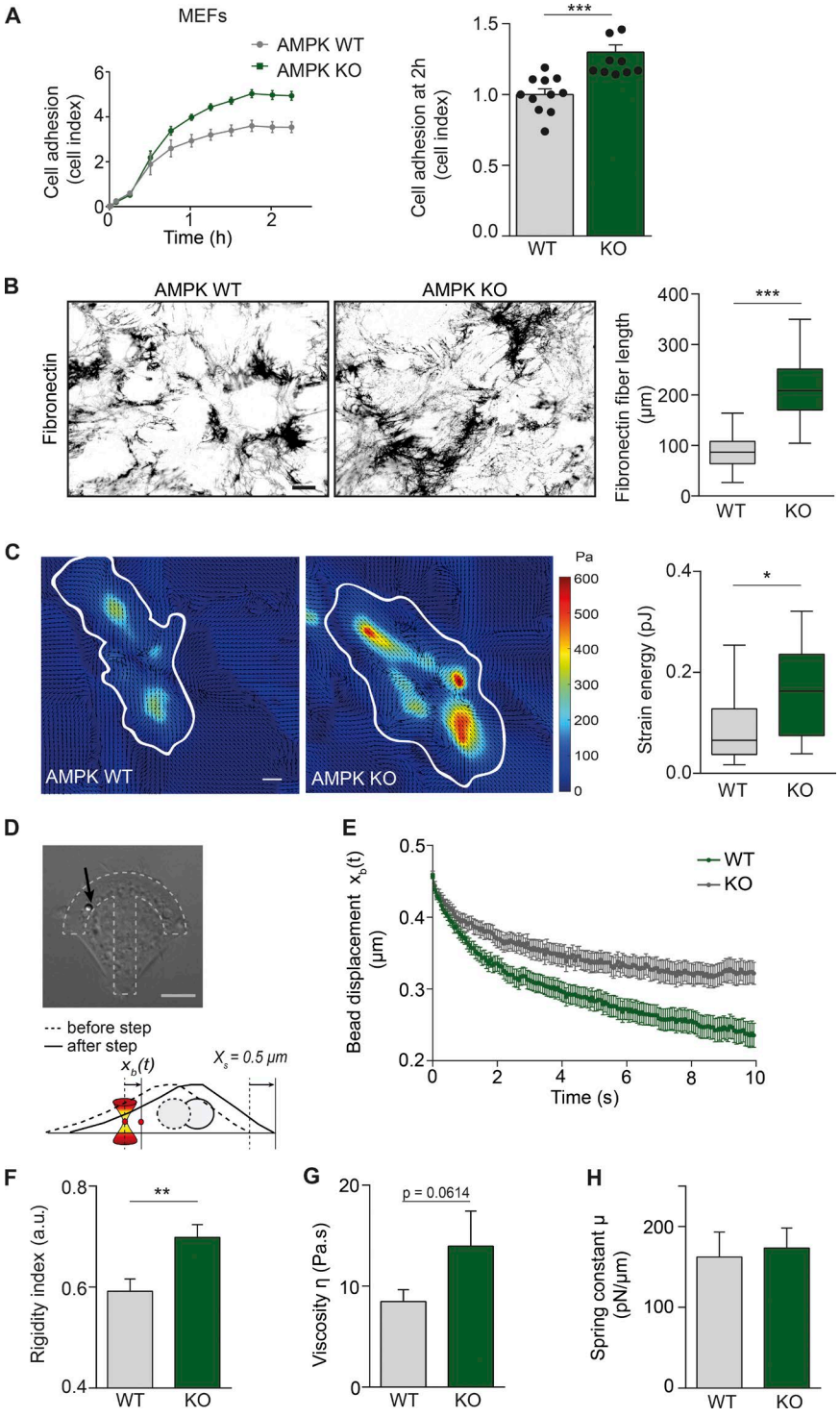

Figure 3. **Loss of AMPK enhances cell adhesion, fibrillogenesis, mechanotransduction, and intracellular stiffness.** (A) Adherence of AMPK WT and KO MEFs on fibronectin measured in real-time using the xCELLigence RTCA instrument. Representative curves of cell adhesion over the first 2 h and quantification of relative cell adhesion (cell index) at 2 h after plating are shown. Data are expressed relative to WT and represent means ± SEM. n = 9–11 experiments from four biological repeats. (B) Representative images and quantification of fibronectin fiber length (µm) in AMPK WT and KO MEFs 16 h after supplementation with 10 µg/ml fibronectin. Data are displayed as Tukey box plots. n > 110 fibers from three biological repeats. (A and B) ***, P < 0.0001 (two-tailed Student's t test). (C) Representative traction force maps and quantification of the mean force (strain energy, pJ) exerted by AMPK WT and KO MEFs plated on fibronectin-coated (5 µg/ml) polyacrylamide gels with a Young's modulus of ∼1 kPa. Black arrows indicate the direction of traction stress. Cell contours are denoted by white lines. The color code gives the magnitude of traction stress in Pa, which corresponds to forces of pN/µm^2. Data are displayed as Tukey box plots. n = 12–14 cells from two biological repeats. *, P = 0.0328 (two-tailed Student's t test). (D) Viscoelastic relaxation experiment in AMPK WT and KO MEFs. Brightfield image of a KO MEF with an internalized 2-µm diameter microsphere (black arrow) plated on a crossbow-shaped micropattern (dotted lines). The schematic depicts the principle of the experiment. The bead is initially trapped using optical tweezers. A step displacement (X_s = 0.5 µm) is then applied to the cell. The displacement of the bead $x_b(t)$ relative to the fixed position of the optical trap is measured. (B–D) Bars: (B) 20 µm; (C and D) 10 µm. (E) Averaged relaxation curves of the bead position after the 0.5-µm step in AMPK WT and KO MEFs. (F–H) Mean values of the rigidity index (F) and of the rheological parameters obtained by fitting the relaxation curves with a SLL model (see the Microrheology in micropatterned cells section of Materials and methods), the intracellular viscosity η (G), and the intracellular spring constant (H) in AMPK WT and KO MEFs. Data shown in E–H are from n = 24 beads from 24 cells from three biological repeats. Error bars represent SEM. **, P = 0.0022 (one-tailed Student's t test). a.u., arbitrary units.

the displacement of an internalized microsphere trapped in optical tweezers (Fig. 3 D; Guet et al., 2014; Mandal et al., 2016). We noted significantly slower viscoelastic relaxation of microspheres in KO compared with WT MEFs (Fig. 3 E), suggesting that the microsphere microenvironment is more resistant to mechanical deformation in the absence of AMPK. Accordingly, AMPK KO MEFs exhibited higher intracellular rigidity (Fig. 3 F) and a trend toward a more viscous environment compared with WT cells when curves were fitted with the standard linear liquid (SLL) model (see the Microrheology in micropatterned cells section of Materials and methods; Fig. 3 G). However, cellular elasticity remained unaltered in the absence of AMPK (Fig. 3 H).

Tensin regulates integrin activity downstream of AMPK

Given that AMPK loss promotes the formation of tensin-rich fibrillar adhesions, we assessed whether AMPK could regulate tensin expression. Of the four tensin family members (tensins1–4), tensin1 and tensin3 contain an integrin-binding (the phosphotyrosine-binding [PTB] domain) and an actin-binding site and localize to fibrillar adhesions (Clark et al., 2010). In

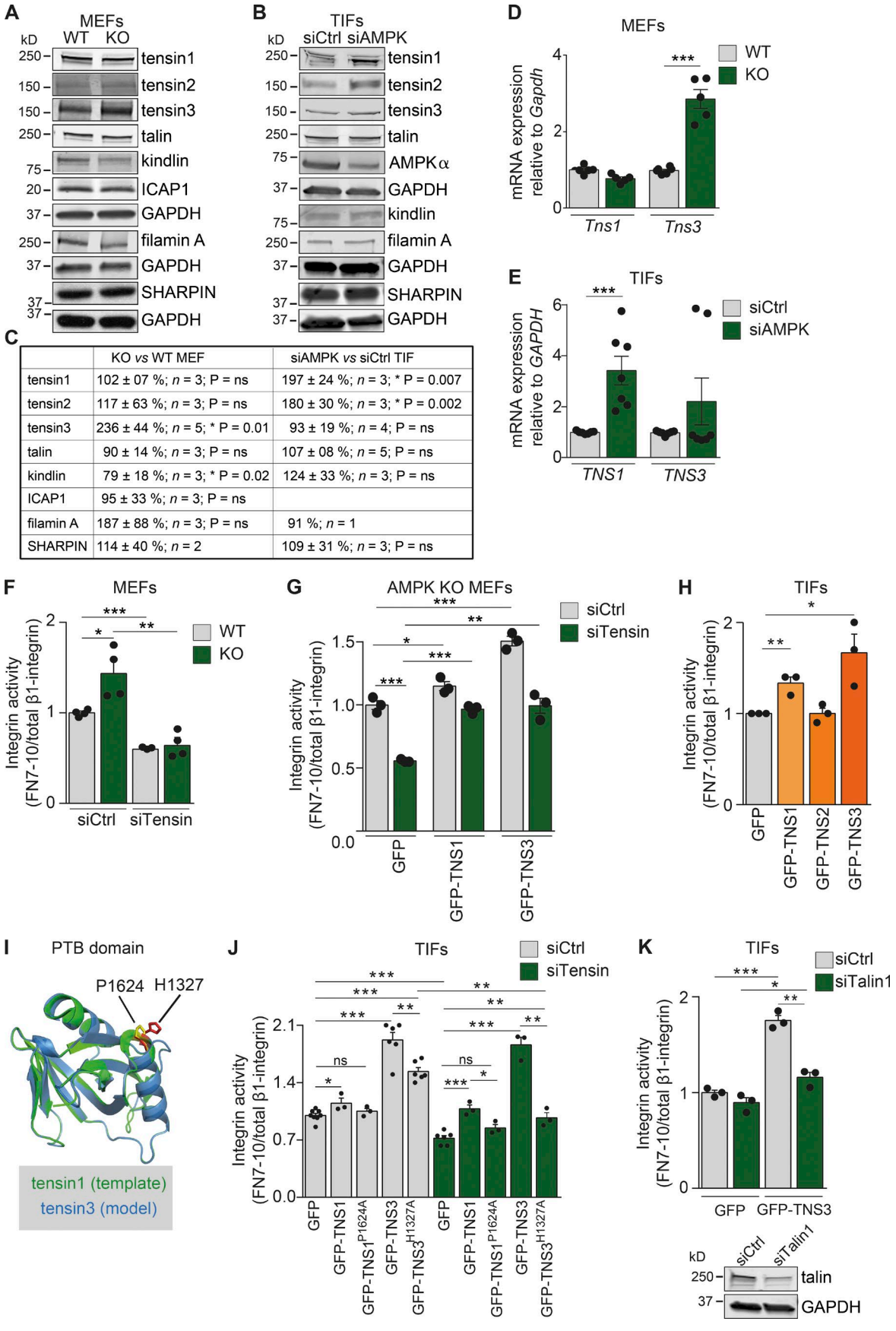

AMPK KO MEFs, tensin3 protein levels were significantly increased compared with WT MEFs (Fig. 4, A and C), whereas the expression of other tensins (tensins1 and 2) and of the known integrin activity regulators, talin, kindlin, ICAP1, filamin A, and SHARPIN, remained unchanged (Fig. 4, A and C). In TIFs, the silencing of AMPK promoted tensin1 and tensin2 protein expression with no alterations in tensin3, talin, kindlin, filamin A, or SHARPIN expression levels (Fig. 4, B and C). In accordance with changes in protein expression, the mRNA levels of tensin3 in AMPK KO MEFs (Fig. 4 D) and tensin1 in siAMPK TIFs (Fig. 4 E) were significantly increased compared with the respective control cells. These data suggest that AMPK regulates the expression of fibrillar adhesion–associated tensins in an isoform- and cell type–dependent manner.

Tensin1 binds the membrane-proximal talin-binding NPxY motif of β-integrin tails through its PTB domain (McCleverty et al., 2007). Nevertheless, the ability of tensin to regulate integrin inside-out activation has not been investigated thus far. To address whether tensins regulate integrin activity downstream of AMPK, we silenced tensin1 (siTensin1) or tensin3 (siTensin3) in AMPK KO MEFs (Fig. S4 A) or AMPK-silenced TIFs (Fig. S4 B), and we observed a significant reduction in integrin activity upon the silencing of either tensin isoform in both cell types. Combined silencing of tensin1 and tensin3 (siTensins1 and 3) decreased integrin activity in AMPK KO MEFs even further than the depletion of the individual tensins (Fig. S4 A), suggesting overlapping functions for tensin1 and tensin3 in the regulation of integrin activity. With this in mind, we decided to proceed with combined tensin1 and 3 silencing in the following experiments. Combined tensin silencing (siTensin) induced a significant reduction in integrin activity in both WT and KO MEFs and, importantly, abolished any difference in integrin activity levels between these cells (Fig. 4 F). Reintroduction of human tensin1 (GFP-TNS1) or human tensin3 (GFP-TNS3) in tensin-silenced AMPK KO MEFs was able to rescue the decrease in integrin activity, and thus the observed effect of tensin siRNAs on integrin activity was not caused by off-target effects (Fig. 4 G). Importantly, overexpression of tensin1 (GFP-TNS1) and, more prominently, tensin3 (GFP-TNS3) significantly increased integrin activity in TIFs (Fig. 4 H) and MEFs (Fig. S4 C), whereas overexpression of the focal adhesion-specific tensin2 did not affect integrin activity in either TIFs or MEFs (Figs. 4 H and S4 C). Collectively, these data demonstrate that tensin1 and tensin3 support β1-integrin activity with possible overlapping and redundant roles.

Direct binding of tensin1 to the β1-integrin tail has been demonstrated previously, and amino acids essential for this interaction have been identified (McCleverty et al., 2007). In particular, alanine (A) substitution of proline P1624 in human tensin1 (GFP-TNS1^{P1624A}) disrupts the tensin1–integrin interaction and the centripetal movement of α5β1-integrin (Rainero et al., 2015). To address whether tensin3, the most potent tensin in supporting integrin activity, also regulates integrins through direct binding to the β1-integrin tail, we generated a point mutation in the PTB domain of tensin3. Based on homology modeling using the established human tensin1 PTB domain (McCleverty et al., 2007), we identified histidine H1327 in the human tensin3 PTB domain as corresponding to P1624 in tensin1 (Fig. 4 I). Based on these analyses, we generated a human tensin3 mutant (GFP-TNS3^{H1327A}), which demonstrated clearly reduced binding to active β1-integrin when compared with tensin3 WT (Fig. S4 D). To assess whether tensin-mediated integrin activation depends on an intact tensin–integrin association, we overexpressed the binding-defective variants GFP-TNS1^{P1624A} and GFP-TNS3^{H1327A} in TIFs silenced for endogenous tensins (siTensin), which are known to form dimers (Lo et al., 1994a). Although GFP-TNS1 and GFP-TNS3 significantly increased integrin activity in the absence of endogenous tensins, GFP-TNS1^{P1624A} was unable to increase integrin activity, and GFP-TNS3^{H1327A} had a very small effect compared with GFP (Fig. 4 J). Collectively, the loss of AMPK promotes the transcriptional activation of the cytoskeletal proteins tensin1 and tensin3, which bind to β1-integrin and support receptor activation.

Next, we investigated whether the ability of tensin to promote integrin activity is independent of talin. To address this question, we overexpressed GFP-TNS3 in the absence of talin1 (siTalin1) and observed that tensin3 could only modestly enhance integrin activity (Fig. 4 K). Based on these data, we hypothesize that integrin activity is triggered by talin1 in focal adhesions and subsequently maintained by tensins in fibrillar adhesions, where talin is mostly absent.

Figure 4. **Tensin regulates integrin activity downstream of AMPK.** (A–C) Immunoblotting (A and B) and quantification (C) of the indicated proteins in WT and AMPK KO MEFs (A and C) and siCtrl or siAMPK TIFs (B and C). GAPDH was used as a loading control. (D and E) Quantification of mRNA levels of *Tns1* and *Tns3* in AMPK WT and KO MEFs relative to the housekeeping genes *Gapdh*, *TNS1*, and *TNS3* in siCtrl and siAMPK TIFs relative to the housekeeping gene *GAPDH* (E). Data are expressed relative to WT (D) and siCtrl (E), respectively, and represent means ± SEM. ***, P < 0.0001 (two-tailed Student's *t* test). (F–H) Quantification of flow cytometric assays of β1-integrin activity assessed as FN7–10 fragment binding relative to total β1-integrin in AMPK WT and KO MEFs (F), AMPK KO MEFs (G), or TIFs (H). (F) AMPK WT and KO MEFs silenced with control siRNA (siCtrl) or with siRNAs against tensin1 and tensin3 (siTensin). Data are expressed relative to WT siCtrl and represent means ± SEM. ***, P < 0.0001 for siTensin WT relative to siCtrl WT; *, P = 0.0216 for siCtrl KO relative to siCtrl WT; and **, P < 0.0029 for siTensin KO relative to siCtrl KO (two-tailed Student's *t* test). (G) siCtrl or siTensin AMPK KO MEFs transiently reexpressing GFP-TNS1, GFP-TNS3, GFP alone in AMPK KO MEFs. Data are expressed relative to siCtrl-GFP–expressing cells and represent means ± SEM. ***, P = 0.0002 for siTensin-GFP relative to siCtrl-GFP; *, P = 0.0399 for siCtrl-TNS1 relative to siCtrl-GFP; ***, P = 0.0006 for siCtrl-GFP-TNS3 relative to siCtrl-GFP; ***, P < 0.0001 for siTensin-GFP-TNS1 relative to siTensin-GFP; and **, P = 0.0019 for siTensin-GFP-TNS3 relative to siTensin-GFP (two-tailed Student's *t* test). (H) TIFs transiently expressing GFP, GFP-TNS1, GFP-TNS2, or GFP-TNS3. Data are expressed relative to GFP and represent means ± SEM. **, P = 0.007 for GFP-TNS1 relative to GFP; and *, P < 0.03 for GFP-TNS3 relative to GFP (two-tailed Student's *t* test). (I) Alignment of the tensin1 PTB domain (1606–1738; Protein Data Bank ID: 1WVH) with the predicted structure of the tensin3 PTB domain. The critical residues for binding β1-integrin are highlighted (yellow for tensin1 and red for tensin3). The amino acids P1624 in tensin1 and H1327 in tensin3 are indicated. (J and K) Quantification of flow cytometric assays of β1-integrin activity assessed as FN7–10 fragment binding relative to total β1-integrin in TIFs. (J) siCtrl or siTensin TIFs transiently expressing GFP, GFP-TNS1, point mutant GFP-TNS1^{P1624A}, GFP-TNS3, and point mutant GFP-TNS3^{H1327A}. Data are expressed relative to siCtrl GFP and represent means ± SEM. For siCtrl cells, *, P = 0.02 for GFP-TNS1 relative to GFP; ***, P < 0.0001 for GFP-TNS3 relative to GFP; ***, P < 0.0001 for GFP-TNS3^{H1327A} relative to GFP; and **, P = 0.004 for GFP-TNS3^{H1327A} relative to GFP-TNS3. For siTensin cells, ***, P = 0.0004 for GFP-TNS1 relative to GFP; ***, P < 0.0001 for GFP-TNS3 relative to GFP; ***, P < 0.0001 for GFP-TNS3^{H1327A} relative to GFP; and **, P = 0.004 for GFP-TNS3^{H1327A} relative to GFP-TNS3. (K) Control or talin1-silenced (siTalin1) TIFs transiently expressing GFP or GFP-TNS3. Data are expressed relative to siCtrl GFP and represent means ± SEM. ***, P = 0.0002 for siCtrl GFP-TNS3 relative to siCtrl GFP; **, P = 0.0013 for siTalin GFP-TNS3 relative to siCtrl GFP-TNS3; *, P = 0.024 for siTalin GFP-TNS3 relative to siTalin GFP (two-tailed Student's *t* test). Below are immunoblots assessing talin expression.

Tensin regulates cell spreading, mechanotransduction, and fibrillogenesis downstream of AMPK

We further sought to explore whether tensin regulates the aforementioned integrin-dependent cellular functions downstream of AMPK. Indeed, tensin1 and tensin3 silencing (siTensin) reduced the amount and the central distribution of active β1-integrin in AMPK KO MEFs plated on fibronectin-coated crossbow-shaped micropatterns (Fig. 5 A). In addition, tensin silencing (siTensin) significantly reduced the spreading of AMPK KO MEFs plated on fibronectin (Fig. 5 B). Finally, tensin silencing reduced both the mechanical stress exerted by AMPK KO MEFs and the remodeling of fibronectin fibers as compared with control-silenced cells (Fig. 5, C and D). To conclude, tensins act downstream of AMPK to regulate integrin activity and localization, cell spreading, mechanotransduction, and fibronectin fibrillogenesis.

Discussion

AMPK is a critical metabolic sensor in cells maintaining energy homeostasis. In recent years, an increasing number of studies demonstrate that AMPK regulates several other cellular functions, such as cell growth and transcription (Mihaylova and Shaw, 2011), cell polarity and cytoskeletal rearrangement (Mirouse and Billaud, 2011), and mitosis (Banko et al., 2011). In this study, starting with unbiased screens (Rantala et al., 2011; Pellinen et al., 2012), we identified AMPK as an integrin activity inhibitor through its ability to negatively regulate the expression of the integrin-binding proteins, tensins. Congruently, loss of AMPK promotes cell adhesion, mechanotransduction, and matrix assembly in fibroblasts (Fig. 6).

Integrin activation by talins and kindlins has been studied extensively; however, the role of other integrin-binding proteins in regulating integrin activity remains elusive. Our data demonstrate that the scaffold protein tensin, known to bind β-integrin at one of the talin-binding sites, supports β1-integrin activity. This is unprecedented, given that other integrin-binding proteins, like DOK-1, which has overlapping binding sites with talin, act as inhibitors of integrin activity (Calderwood et al., 2013). A potential explanation for this finding is that tensins, similar to talin, are among the few proteins that couple integrins to actin (Lo et al., 1994b; Horton et al., 2016), and thus the integrin–tensin complex could extend the list of molecules mediating mechanosensitive coupling of active integrins to actin beyond the well-established integrin-talin-vinculin adhesions.

Fibroblasts adhering to fibronectin generate different types of adhesions, such as nascent, focal, and fibrillar adhesions (Geiger and Yamada, 2011). The first newly formed nascent adhesions transform into focal adhesions and further into fibrillar adhesions under a maturation process that involves force (Geiger and Yamada, 2011). Talins and kindlins are generally absent from fibrillar adhesions, whereas we and others (Clark et al., 2005) have observed high levels of active β1-integrin localizing to these sites. It has been hypothesized earlier—but never shown—that tensin would replace talin in fibrillar adhesions to maintain integrins in an active state (Pylayeva and Giancotti, 2007). Interestingly, we find that tensins induce integrin activity only in conjunction with talin. This suggests that in cells, active integrins may transit from a talin-bound active state to a tensin-maintained active form localizing in fibrillar adhesions. Thus, in this study, we provide concrete evidence for the ability of tensin to support β1-integrin activity, in accordance with the hypothesis of a "talin–tensin switch."

Previous work has demonstrated a critical role for tensins in integrin turnover specifically from fibrillar adhesions (Rainero et al., 2015) and has suggested that integrin and ECM uptake function to provide nutrients under starvation. It is likely that the level of active integrins in fibrillar adhesions is coupled to their endocytic uptake, but the details of this balance and its links to the metabolic state of the cell remain to be explored further.

Integrin adhesion complexes link the ECM to the actin cytoskeleton and mediate force transmission and signaling (Geiger et al., 2001), and thus integrin activity influences the mechanobiology of cells as well. Cell mechanics play a crucial role in cellular functions during development and disease. In this study, we correlate the loss of AMPK with a stiffening of the intracellular environment in agreement with previous work linking β1-integrin levels to the intracellular mechanical state (Baker et al., 2009). Mechanotransduction from the plasma membrane to the cell interior could be mediated by the actin cytoskeleton (Guet et al., 2014; Mandal et al., 2016), which is strongly reorganized upon the loss of AMPK (Fig. 1 D).

An open question remains on how AMPK regulates tensin expression. AMPK is known to directly phosphorylate, and mostly negatively regulate, several transcription factors (Mihaylova and Shaw, 2011). Recently, it was suggested that AMPK can also regulate an array of miRNAs (Liu et al., 2013). Thus, one possibility is that in the absence of AMPK, the transcription factor would translocate to the nucleus and promote tensin expression. Alternatively, an AMPK-regulated miRNA could inhibit tensin expression in cells.

Initially, it might seem paradoxical that a lack of AMPK, a central metabolic regulator, could trigger energy-demanding functions such as matrix remodeling and mechanotransduction. However, the loss of AMPK promotes increased glycolysis (Faubert et al., 2013) to generate ATP and to fuel biosynthesis, and therefore AMPK-deficient fibroblasts are not under energy stress. Interestingly, quiescent fibroblasts, the primary cells that build and maintain the ECM in most soft connective tissues (Humphrey et al., 2014), have increased glycolytic (metabolic) activity associated with enhanced ECM formation (Lemons et al., 2010; Suh et al., 2012).

Fibrillar adhesions are critically important to the most relevant function of fibroblasts in vivo: ECM generation and remodeling. Excessive production of ECM proteins by fibroblasts is linked to many severe human fibrotic conditions, such as chronic kidney disease (Chen et al., 2014a), cardiac hypertrophy (Pelouch et al., 1993), and liver fibrosis (Lim et al., 2012). Recently, AMPK activation has been shown to ameliorate fibrosis in several tissues, and AMPK activators have been suggested as potential therapeutics in the treatment of the aforementioned diseases (Beauloye et al., 2011; Satriano et al., 2013). Our data demonstrating that AMPK inhibition induces fibrillar adhesions, integrin activity, and the ability of fibroblasts to modify ECM composition via fibronectin fibrillogenesis provide important mechanistic insight into the link between AMPK and fibrosis. Currently, the clinical relevance of tensins in fibrotic conditions linked to AMPK activity is not known, and this will be an interesting area of research in the future.

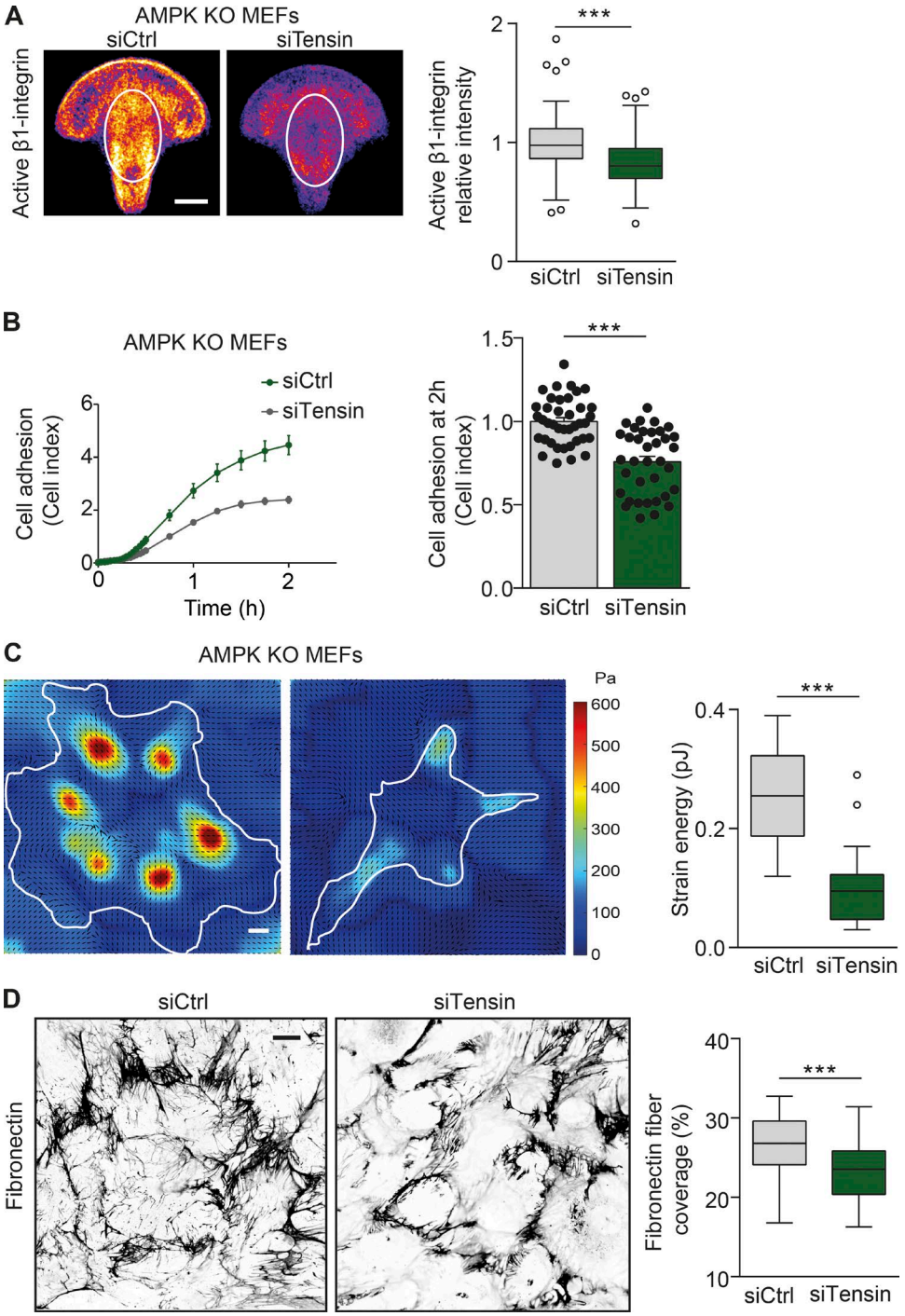

Figure 5. **Tensin regulates cell spreading, mechanotransduction, and fibrillogenesis downstream of AMPK.** (A) Representative mean intensity maps of bottom-plane images obtained with a spinning-disk confocal microscope. siCtrl or siTensin AMPK KO MEFs are stained for active β1-integrin (9EG7) and plated on fibronectin-coated crossbow-shaped micropatterns. The mean active β1-integrin distribution is represented with a heat map, wherein yellow corresponds to regions within the cell containing the largest accumulation of active β1-integrin. The white ovals indicate the centrally located adhesions, and the level of active β1-integrin within the ovals was quantified and displayed as Tukey box plots. $n > 70$ cells from four biological repeats. (B) Adherence of siCtrl and siTensin AMPK KO MEFs on fibronectin (1 µg/ml) as measured in real time using the xCELLigence RTCA instrument. Quantification of relative cell adhesion (cell index) at 2 h after plating is shown. Data are expressed relative to siCtrl and represent means ± SEM. $n > 35$ from 12 independent experiments. (C) Representative traction force maps and quantification of the mean force (strain energy, pJ) exerted by siCtrl and siTensin AMPK KO MEFs plated on fibronectin-coated (5 µg/ml) polyacrylamide gels with a Young's modulus of ~3 kPa. Black arrows indicate the direction of traction stress. Cell contours are denoted by white lines. The color code gives the magnitude of traction stress in Pa, which corresponds to forces of pN/µm^2. Data are displayed as Tukey box plots. n = 18–19 cells from three biological repeats. (D) Representative confocal images obtained with a spinning-disk confocal microscope and quantification of the area covered by fibronectin in siCtrl and siTensin AMPK KO MEFs 16 h after supplementation with 10 µg/ml fibronectin. Data are displayed as Tukey box plots. $n > 70$ images from three biological repeats. (A, C, and D) Bars: (A and C) 10 µm; (D) 20 µm. (A–D) ***, $P < 0.0001$ (two-tailed Student's t test).

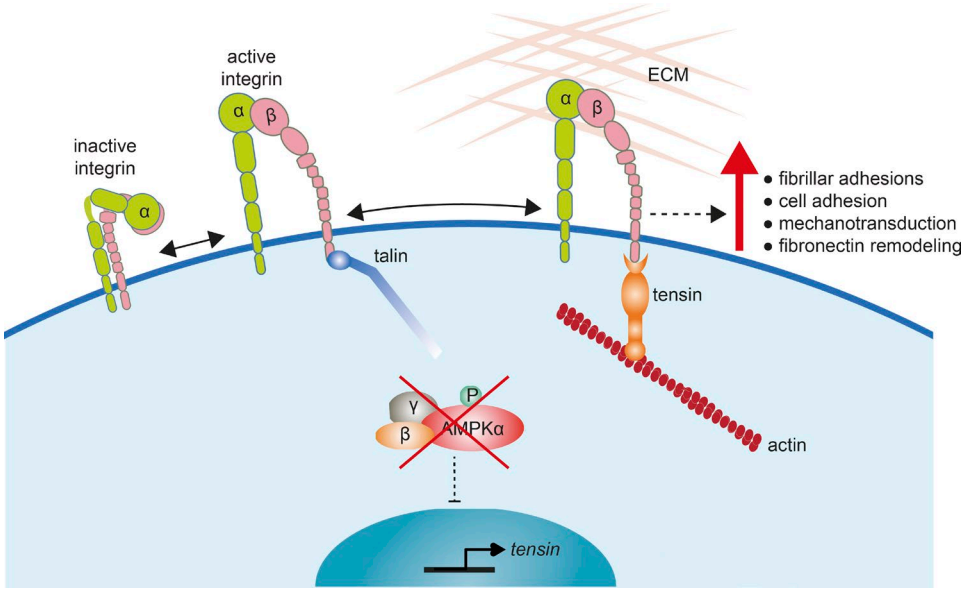

Figure 6. **Model showing how AMPK loss promotes tensin-mediated integrin activity.** In the absence of AMPK, the transcriptional constraints that limit tensin expression are removed. A corresponding increase in tensin expression leads to enhanced tensin binding to β1-integrin tails to support integrin activity after initial integrin activation by talin. This leads to enhanced fibrillar adhesion formation and integrin-dependent processes such as mechanotransduction and fibronectin remodeling. P, phosphorylated.

Materials and methods

MEF isolation and cell culture

To generate immortalized MEFs, pregnant female mice were maintained in the University of Helsinki's Laboratory Animal Center, and MEF isolation was approved by the National Animal Experiment Board in Finland. AMPKα1$^{+/-}$;α2$^{lox/lox}$ and AMPKα1$^{-/-}$;α2$^{lox/lox}$ MEFs were isolated from E12.5 embryos and immortalized at passage 2 using the carboxy terminus of p53 in pBabe-Hygro57 and 200 mg/ml hygromycin selection for 7 d (Yan et al., 2015). MEFs were then transduced with adenoviral vectors expressing GFP to obtain immortalized AMPKα1$^{+/-}$;α2$^{+/+}$ (WT) and AMPKα1$^{-/-}$;α2$^{+/+}$ (α1KO) or Cre recombinase to obtain immortalized AMPKα1$^{+/-}$;α2$^{-/-}$ (α2KO) and AMPKα1$^{-/-}$;α2$^{-/-}$ (KO) MEFs. MEFs were cultured in DMEM 4500 (Sigma-Aldrich) supplemented with 10% FBS (Gibco), 2 mM L-glutamine (Sigma-Aldrich), and 1 mM pyruvate. Human TIFs were a gift from J. Norman (Beatson Institute, Glasgow, Scotland, UK) and were cultured in DMEM 4500 supplemented with 20% FBS, 2 mM L-glutamine, and 20 mM Hepes buffer (Sigma-Aldrich). HEK293 cells were grown in DMEM 4500 supplemented with 10% FBS and 2 mM L-glutamine. All cells were routinely tested for mycoplasma contamination.

siRNA and plasmid transfections

siRNA silencing was performed using 20 nM siRNA oligonucleotides and Lipofectamine RNAiMAX reagent (Thermo Fisher Scientific) according to the manufacturer's protocol, and cells were cultured for 3 d. The siRNAs used for simultaneous AMPKα1 and AMPKα2 silencing were PRKAA1 (sc-29673), PRKAA2 (sc-38923), and control (sc-37007; Santa Cruz Biotechnology, Inc.; Wang et al., 2012). The additional siRNAs against AMPKα1 were from Integrated DNA Technologies (siRNA 1: 151509037; and siRNA 2: 151509031). The siRNAs against mouse Prkaa1 (L-041035; smartpool), mouse Prkaa2 (L-040809; smartpool), mouse Tns1 (L-040925; smartpool), mouse Tns3 (L-063982; smartpool; and J-063982-08; individual), human tensin1 (L-009976; smartpool), human tensin3 (L-009997; smartpool), and control (D-001810-10; nontargeting pool) were ON-TARGETplus siRNAs from Thermo Fisher Scientific. The siRNA against human talin1 was Hs_TLN1_2 FlexiTube (SI00086968), and the negative control used was the AllStars Negative Control (SI03650318) from QIAGEN. Sequences of all the siRNAs used are provided in the Table S1. Lipofectamine 3000 and P3000TM Enhancer reagent (Thermo Fisher Scientific) were used for transient plasmid transfections according to the manufacturer's protocol, and the cells were cultured for 24 h. Transient overexpressions in previously silenced cells were performed 72–96 h after siRNA transfection, when the endogenous tensin protein levels were still reduced but no effective siRNA was present anymore.

GFP-TNS1 and GFP-TNS3 constructs were generated by inserting SalI-digested sequences into pEGFP-C1 vectors cut with XhoI and HindIII enzymes (Takara Bio Inc.; Clark et al., 2010). GFP-TNS1^{P1624A} was a gift from J. Norman. GFP-TNS3-H1327→A site-directed point mutation was introduced using the QuikChange II XL Site-directed Mutagenesis kit (Agilent Technologies) according to the manufacturer's instructions. The primers used were forward, 5′-CCCTCACCG GCGCCCAGGCGATCCAGAAGGCCC-3′, and reverse, 5′-CCTTCT GGATCGCCTGGGCGCCGGTGAGGGACTCC-3′. All constructs were validated with sequencing.

Antibodies, compounds, and reagents

The following antibodies were used in the study: rabbit (rbt) anti–phosphorylated acetyl-CoA carboxylase (ACC; 3662), rbt anti-ACC (3661), rbt anti-AMPK (2532), rbt anti–filamin A (4762; Cell Signaling Technology), rbt anti-tensin1 (Sab4200283), rbt anti-tensin2 (SAB4200161), rbt anti-fibronectin (F3648), mouse (ms) anti-talin1 (clone 8d4; T3287; Sigma-Aldrich), rbt anti-tensin3 (Rb33; gift from K. Clark, University of Leicester, Leicester, England, UK; Clark et al., 2010), rbt anti–β1-integrin tail (clone EP1041Y; Ab52971), ms anti–human active β1-integrin (clone 12G10; Ab30394), rbt anti-kindlin (ab68041), ms anti-GFP (clone 9F9.F9; Ab1218; Abcam), rat anti–mouse active β1-integrin (clone 9EG7; 553715; BD), rat anti–mouse total β1-integrin (clone MB1.2; MAB1997; EMD Millipore), ms anti–human total β1-integrin (clone P5D2; Developmental Studies Hybridoma Bank), rbt anti-paxillin (H114; sc5574; Santa Cruz Biotechnology, Inc.), rbt anti-SHARPIN

(bs-9581R; Bioss Inc.), ms anti–human active α5-integrin (SNAKA51; gift from M. Humphries, University of Manchester, Manchester, England, UK; Clark et al., 2005), rbt anti-ICAP1 (gift from D. Bouvard, Centre National de la Recherche Scientifique, Paris, France), and ms anti-GAPDH (5G4; Mab6C5; HyTest). Phalloidin Atto 647N (65906) was obtained from Sigma-Aldrich. Alexa Fluor–conjugated secondary antibodies (Alexa Fluor 488–, 555–, and 647–conjugated anti–mouse, –rabbit, and –rat antibodies; Thermo Fisher Scientific) were used in immunofluorescence and flow cytometry. Bovine plasma fibronectin (341631) was purchased from EMD Millipore, and dorsomorphin (S7306; dissolved in DMSO) was obtained from Selleckchem.

Western blot

Protein extracts were separated using SDS-PAGE under denaturing conditions (4–20% Mini-PROTEAN TGX Gels) and were transferred to the nitrocellulose membrane (Bio-Rad Laboratories). Membranes were blocked with 5% milk-TBST (Tris-buffered saline and 0.1% Tween 20), incubated with the indicated primary antibodies overnight at 4°C, and then incubated with fluorophore-conjugated or ECL HRP-linked secondary antibodies (GE Healthcare) at RT for 1 h. Membranes were scanned using an infrared imaging system (Odyssey; LI-COR Biosciences) or ECL Plus Western blotting reagent (GE Healthcare), and film was developed. Band intensity was determined using Fiji (ImageJ; National Institutes of Health; Schindelin et al., 2012).

Flow cytometry assays for β1-integrin activity

For the flow cytometry assay using labeled FN7–10 binding as a readout of cell surface active β1-integrin levels, cells were detached using trypsin, washed once with full medium containing 10% FBS, and resuspended in 100 µl of 37°C serum-free medium with (a) 10 µg/ml Alexa Fluor 647–conjugated FN7–10, (b) 30 µg/ml FN7–10 supplemented with 5 mM EDTA (the negative control), or (c) total β1-integrin antibody (P5D2 for human cells or 10 µg/ml MB1.2 for mouse cells) and 10 µg/ml Alexa Fluor 647–conjugated secondary antibody. Cells were incubated with rotation for 45 min at RT. After washing once with cold Tyrode's buffer (10 mM Hepes-NaOH, pH 7.5, 137 mM NaCl, 2.68 mM KCl, 0.42 mM NaH_2PO_4, 1.7 mM $MgCl_2$, 11.9 mM $NaHCO_3$, 5 mM glucose, and 0.1% BSA), cells were fixed with 4% PFA in PBS for 10 min at RT, and fluorescence was measured by flow cytometry (FACSCalibur, LSRFortessa, or LSRII; BD). The Geomean fluorescent intensity was measured from 5,000–20,000 events. Viable single cells were gated by forward scatter and side scatter dot blots (2.5.1; Flowing Software). In experiments using GFP constructs, the GFP-expressing cells were gated and analyzed for allophycocyanin (647) intensity. Flow cytometric analysis of active β1-integrin cell surface levels using conformation-specific antibodies was performed in PFA-fixed cells. Cells were washed with cold Tyrode's buffer and stained with active β1-integrin specific antibody (5 µg/ml 9EG7 for human/mouse cells) or total β1-integrin antibody (P5D2 for human and MB1.2 for mouse cells) for 1 h at 4°C (Nevo et al., 2010). Cells were washed with Tyrode's buffer and incubated with fluorescently conjugated secondary antibodies (6 µg/ml) for 1 h at 4°C. The negative control cells were stained only with secondary antibody. All antibodies were diluted into Tyrode's buffer. Fluorescence was measured by flow cytometry (FAC SCalibur or LSRFortessa).

Adhesion assay using xCELLigence real-time cell analysis (RTCA)

The xCELLigence RTCA instrument (Roche) was used to measure cell adhesion over time. RTCA measures impedance between electrodes (bottom sensors) expressed as cell index values. The 96-well E-plate (Roche) was coated with 1 µg/ml fibronectin or 5 µg/ml vitronectin (A14700; Thermo Fisher Scientific) in PBS, followed by blocking with 0.1% BSA in PBS, both at 37°C for 1 h. The cells were detached and washed with full medium containing 10% FBS, and 10,000 cells/well were seeded on E-plates in serum-free medium. Cell index was measured in real time.

Fibronectin fibrillogenesis

50,000 cells were plated on coverslips and allowed to adhere for 4 h. After the addition of exogenous 10 µg/ml fibronectin, cells were incubated for a further 16 h and then fixed with 4% PFA. Cells were stained with anti-fibronectin (5 µg/ml), phalloidin (1:200), and DAPI (0.5 µg/ml; nuclei staining) in PBS. The length of individual fibers was determined manually in ImageJ. To assess fibronectin coverage, the images were processed with fast Fourier transform bandpass filters to visualize all fibers, and the amount of fibronectin was measured by thresholding using Fiji (Schindelin et al., 2012).

Microscopy

Confocal images were acquired with a spinning-disk confocal microscope (Marianas spinning-disk imaging system [Intelligent Imaging Innovations, Inc.] with a CSU-W1 scanning unit [Yokogawa Electric Corporation] on an inverted Axio Observer Z1 microscope [ZEISS]) using a 63×, 1.4 N.A. Oil Plan-Apochromat M27 with a differential interference contrast III Prism or a 100×, 1.4 N.A. Oil Plan-Apochromat M27 objective and an Orca Flash 4 sCMOS camera (Hamamatsu Photonics), and software used was Slidebook 6 (Intelligent Imaging Innovations, Inc.). Fixed samples were mounted with Mowiol 4–88 (475904; EMD Millipore) containing 2.5% 1,4-diazobicyclo-[2.2.2]-octane (D27802; Sigma-Aldrich) and imaged at RT. The fluorescence intensity and the coverage of the antibody staining were quantified by thresholding using Fiji and normalized to cell area.

Images with a TIRF microscope (Laser-TIRF 3 Imaging System; ZEISS) were acquired using a 63×, 1.46 N.A. Oil α Plan-Apochromat differential interference contrast or a 100×, 1.46 N.A. Oil α Plan-Apochromat differential interference contrast objective and an electron-multiplying charge-coupled device camera (ImageEM C9100-13; Chip size, 512 × 512; Hamamatsu Photonics) controlled by the Zen software (Zen 2012 Blue Edition Systems; ZEISS). Fixed TIRF samples were kept in PBS during imaging and were imaged at RT. Quantitative analysis for images was performed using Fiji.

Micropatterns and immunostaining

Micropatterns were produced on glass coverslips (Azioune et al., 2009; Alanko et al., 2015). Glass coverslips were cleaned with 97% ethanol, dried with airflow, and exposed to deep UV light for 5 min. The clean coverslips were placed upside down on parafilm containing 0.1 mg/ml poly(L-lysine)-graft-poly(ethylene glycol) (Surface Solutions) in 10 mM Hepes, pH 7.3, and incubated for 1 h at RT. They were then rinsed once with PBS and once with water, dried, and stored on the bench. Crossbow-shaped 45-µm micropatterns were designed on a chromium synthetic quartz photomask (Delta Mask B.V.). The photomask was cleaned once with water and twice with 97% ethanol, dried with airflow, and exposed to deep UV light for 5 min. Small drops of water were pipetted on the clean photomask, and the pegylated coverslips were placed on top. The photomask with the coverslips facing down were placed in the UV oven for 6 min. The coverslips were removed from the photomask with water, dried, and coated with 50 µg/ml fibronectin and 5 µg/ml fibrinogen Alexa Fluor 647 for 1 h at RT. The coverslips were placed in 12-well plates and incubated with medium without antibiotics containing 20 mM Hepes at 37°C for 5 min. The cells were then trypsinized, and 100,000 cells were plated, left to adhere for 10 min at 37°C, washed with medium to remove nonadherent cells, and incubated for another 7 h in culture medium containing Hepes before fixing with

4% PFA. Alternatively, cells were plated on 5 µg/ml fibronectin–coated glass-bottom dishes (MatTek Corporation) for 7 h and fixed with 4% PFA. Samples were washed, permeabilized with 0.5% Triton-X for 10 min, blocked with 1 M glycine for 30 min, washed, and incubated with the indicated primary antibodies for another 30 min. After further washes, cells were incubated with Alexa Fluor–conjugated secondary antibodies (6 µg/ml), 647N-phallodin (1:200), and 0.5 µg/ml DAPI in PBS for 30 min. For Mn^{2+} treatment, adherent cells were incubated for 2 h with 2 mM Mn^{2+} before fixation. Finally, cells were washed and imaged with a TIRF or spinning-disk confocal microscope.

Traction force microscopy (TFM)

Preparation of hydrogels. Glass coverslips (P35G-1.0-14-C; MatTek Corporation) were treated with 100 µl Bind Silane solution (a mixture of 714 µl PlusOne Bind Silane [Silane A-174; GE Healthcare], 714 µl acetic acid, and 96% ethanol [≤10 ml]) for 10 min at RT. The glass was washed twice with ethanol and once with mQH_2O and was left to dry completely. A mixture of 150 µl of 40% acrylamide (A4058; Sigma-Aldrich), 50 µl of 2% *N*, *N*′-methylenebisacrylamide solution (M1533; Sigma-Aldrich), 300 µl PBS, and 3.4 µl of sonicated 0.2-µm FluoroSphere beads (505/515; F881; Thermo Fisher Scientific) was preprepared and vortexed briefly. Gel polymerization was initiated by the addition of 1 µl of Temed (T9281; Sigma-Aldrich) and 5 µl of 10% ammonium persulfate to the acrylamide mix. After quick vortexing, 11.7 µl of this mixture was pipetted onto the glass plates, a round 13-mm coverslip was carefully placed on top of the drop so that a thin layer of liquid remained between the two glass surfaces, and the mixture was incubated for 1 h. PBS was then added to cover the entire dish, and the glass coverslip was carefully removed. This protocol of hydrogel preparation achieved a Young's modulus of ∼3 kPa. For functionalization, 0.2 mg/ml sulfo-SANPAH (22589; Thermo Fisher Scientific) and 2 mg/ml *N*-(3-dimethylaminopropyl)-*N*′-ethylcarbodiimide hydrochloride (EDC; 03450; Sigma Aldrich) in 50 mM Hepes were added on top of formed gels and incubated for 30 min at RT with gentle agitation. Gels were put into a UV chamber for 10 min without cover to activate the sulfo-SANPAH and finally were washed three times with PBS before overnight coating with fibronectin at 4°C.

Image acquisition and TFM analysis. Cells were plated onto TFM plates 24 h before the experiment. For imaging, we used an LSM780 laser-scanning confocal microscope and a 63×, 1.2 W C Apochromat objective (ZEISS). The cells were maintained in their culture medium during imaging and were imaged live at 37°C. A fluorescence image of the beads (Excitation, 488 nm; Detection, 500–550 nm) and a phase-contrast image of the colonies were recorded for 7–10 colonies per sample. To ensure good-quality imaging of fluorescent beads, we performed Z stacks of 11 images with a separation of 1 µm and then manually chose the best focus. After the first round of images, cells were removed by the addition of an extraction buffer (20 mM NH_4OH and 0.5% Triton-X in PBS). At this point, reference images for each of the 7–10 locations, now without cells, were recorded in the exact same way as images acquired with the cells. To extract the bead displacement fields, we used a MATLAB software package (MathWorks) provided by T. Betz (University of Münster, Münster, Germany) that uses a correlation algorithm described previously (Betz et al., 2011). Traction forces were determined using the same MATLAB software package after the Fourier transform traction force algorithm, as introduced by Butler et al. (2002).

Microrheology in micropatterned cells

Active microrheology based on optical tweezers was performed in crossbow-shaped micropatterned cells (Guet et al., 2014; Mandal et al., 2016). In brief, 2-µm-diameter fluorescent microspheres (Thermo Fisher Scientific) were allowed to internalize in cells overnight. Cells were then detached and allowed to readhere for 2 h on 38-µm-diameter crossbow-shaped micropatterns coated with 5 µg/ml fibronectin. The culture medium was supplemented with 20 mM Hepes before experimental manipulations on an A1R confocal microscope (Nikon) equipped with a 37°C incubator, a nanometric piezostage (Mad City Labs), and a homemade single fixed optical trap (1,060–1,100 nm; 2-W maximal output power; IPG Photonics). A bead was trapped by optical tweezers (1-W laser output power, corresponding to 150 mW on the sample), and after a 0.5-µm step displacement of the stage applied by the piezostage, the bead relaxation $x_b(t)$ toward the optical trap center was measured using single particle tracking. First, a model-independent phenomenological parameter, the rigidity index, was calculated as the normalized area under the relaxation curve (Mandal et al., 2016). Second, the SLL model (Bausch et al., 1999; Chan et al., 2015; Mandal et al., 2016) was used to fit the relaxation curves. The SLL model consists of a Kelvin–Voigt body (a spring of spring constant µ and a dashpot of viscosity η in parallel) and a dashpot in series.

Quantitative real-time PCR

Total cellular RNA was extracted using the NucleoSpin RNA kit (MACHEREY-NAGEL), and 1 µg of the extracted RNA was used as a template for cDNA synthesis by the high-capacity cDNA reverse transcription kit (Applied Biosystems) according to the manufacturer's protocol. Expression levels of human and mouse Tensin1 and Tensin3 were determined by TaqMan quantitative real-time PCR using the RT-PCR HT7900 (Applied Biosystems). The expression level of GAPDH was used as a reference (endogenous control). TaqMan Universal Master Mix II included necessary components for quantitative RT-PCR reactions. The following primers from Sigma-Aldrich were used for human samples: human *TNS1* (forward, 5′-CCAGACACCCACCTG ACTTAG-3′, and reverse, 5′-CAGCTCATGGTTGGATGGA-3′; Universal ProbeLibrary probe 82), human *TNS3* (forward, 5′-AGGCTG CCTGACACAGGA-3′, and reverse, 5′-AGGGGCTGTTCAGCA GAG-3′; Universal ProbeLibrary probe 57), and human *GAPDH* (forward, 5′-GCTCTCTGCTCCTCCTGTTC-3′, and reverse, 5′-ACG ACCAAATCCGTTGACTC-3′; probe 60). The following primers from Sigma-Aldrich were used for mouse samples: mouse *Tns1* (forward, 5′-GACAAGATCGTGCCCATTG-3′, and reverse, 5′-CCAGAGAGT AGGCCACTGAAG-3′; Universal ProbeLibrary probe 82) and mouse *Tns3* (forward, 5′-TCCGTTCAGTCCACCTGAG-3′, and reverse, 5′-ATCTCTGGGCAGCCTCGT-3′; Universal ProbeLibrary probe 20); mouse *Gapdh* primers and probes were from Universal ProbeLibrary. Relative expression was calculated by the 2ΔΔCT method using the expression level of GAPDH as a reference for the quantification.

Immunoprecipitation

HEK293 cells were transiently transfected with expression constructs coding for pEGFP-C1, GFP-TNS3, and GFP-TNS3 with H1327A mutation. Cells were lysed (0.5% Triton X-100, 10 mM Pipes, pH 6.8, 150 mM NaCl, 150 mM sucrose, 3 mM $MgCl_2$, cOmplete, and phosphatase inhibitors [Mediq; Roche]), cleared by centrifugation, and incubated with antibody-coated protein G magnetic beads (1 µg of antibody per 10 µl of beads; Dynabeads; Thermo Fisher Scientific) for 1 h at 4°C. Complexes bound to the beads were isolated using magnets, washed three times with ice-cold lysis buffer, and eluted in reducing sample buffer (Jacquemet et al., 2013). Input and precipitate samples were analyzed by Western blotting.

Homology modeling of TNS3 PTB domain

The TNS3-PTB domain (1309–1439) was modeled using a Swiss-Model server and the TNS1-PTB domain (1606–1738; Protein Data

Bank ID: 1WVH) as a template. Then, pairwise structure superimposition of TNS3-PTB and TNS1-PTB was performed using Molecular Graphics Systems software (1.7.4.4 Edu; PyMOL).

Statistical analysis

Statistical significance was determined using the unpaired two-tailed Student's *t* test unless otherwise indicated. All experiments were repeated at least three times unless otherwise indicated. Data distribution was assumed to be normal, but this was not formally tested. *n* numbers are indicated in the graphs as black dots or in the figure legends. A p-value of 0.05 was considered to be a borderline for statistical significance. P-values are indicated in the figure legends. Tukey box plots show the 25th–75th percentiles delineated by the upper and lower limits of the box, the median is shown by the horizontal line inside the box, whiskers extend to data points that are >1.5× interquartile range away from first/third quartile, and outliers are represented by open circles.

Online supplemental material

Fig. S1 shows that AMPK negatively regulates β1-integrin activity. Fig. S2 shows that AMPK depletion promotes fibrillar adhesion formation. Fig. S3 shows that loss of AMPK enhances cell adhesion, fibrillogenesis, mechanotransduction, and intracellular stiffness. Fig. S4 shows that tensin regulates integrin activity downstream of AMPK. Table S1, included as an Excel file, is a list of siRNA sequences used in this study.

Acknowledgments

We thank P. Laasola and J. Siivonen for technical assistance, M. Saari for help with the microscopes, H. Hamidi for editing of the manuscript, J. Alanko for the micropatterns, J. Pouwels for critical comments on the manuscript, and the Cell Imaging Core facility at the University of Turku Centre for Biotechnology for help with imaging. Professor B. Goud is acknowledged for support and intellectual input in the study. Part of the study was carried out by J. Ivaska related to the LaBex CelTisPhyBio International Chair program at Institute Curie.

This study has been supported by the Academy of Finland, the Sigrid Juselius Foundation, and the Cancer Society of Finland (to J. Ivaska and T.P. Mäkelä) and by a European Research Council Consolidator (grant 615258 to J. Ivaska). M. Georgiadou and G. Jacquemet are supported by a European Molecular Biology Organization Long-Term Fellowship. J. Lilja and P. Sahgal are supported by the University of Turku Doctoral Program of Molecular Medicine. Y. Yan is supported by the Doctoral Program in Biomedicine and the Finnish Cultural Foundation. C. Alibert and J.-B. Manneville were supported by grants from Université Pierre et Marie Curie University Paris 6 (Program Doctoral Interfaces Pour le Vivant) and from the Plan Cancer 2012 Institut National de la Santé et de la Recherche Médicale–Tecsan grant PC201125.

The authors declare no competing financial interests.

Author contributions: Conceptualization, M. Georgiadou and J. Ivaska; methodology, M. Georgiadou, J. Lilja, G. Jacquemet, C. Guzmán, J.-B. Manneville, and J. Ivaska; investigation, M. Georgiadou, J. Lilja, G. Jacquemet, C. Guzmán, M. Rafaeva, C. Alibert, P. Sahgal, M. Lerche, and J. Ivaska; resources, Y. Yan, T.P. Mäkelä, and J. Ivaska; writing—original draft, M. Georgiadou; writing—reviewing, M. Georgiadou, G. Jacquemet, and J. Ivaska; visualization, M. Georgiadou; supervision, J.-B. Manneville and J. Ivaska; funding acquisition, J. Ivaska.

Submitted: 15 September 2016
Revised: 20 December 2016
Accepted: 3 February 2017

References

Alanko, J., A. Mai, G. Jacquemet, K. Schauer, R. Kaukonen, M. Saari, B. Goud, and J. Ivaska. 2015. Integrin endosomal signalling suppresses anoikis. *Nat. Cell Biol.* 17:1412–1421. http://dx.doi.org/10.1038/ncb3250

Askari, J.A., C.J. Tynan, S.E. Webb, M.L. Martin-Fernandez, C. Ballestrem, and M.J. Humphries. 2010. Focal adhesions are sites of integrin extension. *J. Cell Biol.* 188:891–903. http://dx.doi.org/10.1083/jcb.200907174

Azioune, A., M. Storch, M. Bornens, M. Théry, and M. Piel. 2009. Simple and rapid process for single cell micro-patterning. *Lab Chip.* 9:1640–1642. http://dx.doi.org/10.1039/b821581m

Baker, E.L., R.T. Bonnecaze, and M.H. Zaman. 2009. Extracellular matrix stiffness and architecture govern intracellular rheology in cancer. *Biophys. J.* 97:1013–1021. http://dx.doi.org/10.1016/j.bpj.2009.05.054

Banko, M.R., J.J. Allen, B.E. Schaffer, E.W. Wilker, P. Tsou, J.L. White, J. Villén, B. Wang, S.R. Kim, K. Sakamoto, et al. 2011. Chemical genetic screen for AMPKα2 substrates uncovers a network of proteins involved in mitosis. *Mol. Cell.* 44:878–892. http://dx.doi.org/10.1016/j.molcel.2011.11.005

Bausch, A.R., W. Möller, and E. Sackmann. 1999. Measurement of local viscoelasticity and forces in living cells by magnetic tweezers. *Biophys. J.* 76:573–579. http://dx.doi.org/10.1016/S0006-3495(99)77225-5

Beauloye, C., L. Bertrand, S. Horman, and L. Hue. 2011. AMPK activation, a preventive therapeutic target in the transition from cardiac injury to heart failure. *Cardiovasc. Res.* 90:224–233. http://dx.doi.org/10.1093/cvr/cvr034

Betz, T., D. Koch, Y.B. Lu, K. Franze, and J.A. Käs. 2011. Growth cones as soft and weak force generators. *Proc. Natl. Acad. Sci. USA.* 108:13420–13425. http://dx.doi.org/10.1073/pnas.1106145108

Bouvard, D., J. Pouwels, N. De Franceschi, and J. Ivaska. 2013. Integrin inactivators: balancing cellular functions in vitro and in vivo. *Nat. Rev. Mol. Cell Biol.* 14:430–442. http://dx.doi.org/10.1038/nrm3599

Butler, J.P., I.M. Tolić-Nørrelykke, B. Fabry, and J.J. Fredberg. 2002. Traction fields, moments, and strain energy that cells exert on their surroundings. *Am. J. Physiol. Cell Physiol.* 282:C595–C605. http://dx.doi.org/10.1152/ajpcell.00270.2001

Byron, A., J.D. Humphries, J.A. Askari, S.E. Craig, A.P. Mould, and M.J. Humphries. 2009. Anti-integrin monoclonal antibodies. *J. Cell Sci.* 122:4009–4011. http://dx.doi.org/10.1242/jcs.056770

Byron, A., J.A. Askari, J.D. Humphries, G. Jacquemet, E.J. Koper, S. Warwood, C.K. Choi, M.J. Stroud, C.S. Chen, D. Knight, and M.J. Humphries. 2015. A proteomic approach reveals integrin activation state-dependent control of microtubule cortical targeting. *Nat. Commun.* 6:6135. http://dx.doi.org/10.1038/ncomms7135

Calderwood, D.A., I.D. Campbell, and D.R. Critchley. 2013. Talins and kindlins: partners in integrin-mediated adhesion. *Nat. Rev. Mol. Cell Biol.* 14:503–517. http://dx.doi.org/10.1038/nrm3624

Chan, C.J., A.E. Ekpenyong, S. Golfier, W. Li, K.J. Chalut, O. Otto, J. Elgeti, J. Guck, and F. Lautenschläger. 2015. Myosin II activity softens cells in suspension. *Biophys. J.* 108:1856–1869. http://dx.doi.org/10.1016/j.bpj.2015.03.009

Chen, K.H., H.H. Hsu, C.C. Lee, T.H. Yen, Y.C. Ko, C.W. Yang, and C.C. Hung. 2014a. The AMPK agonist AICAR inhibits TGF-β1 induced activation of kidney myofibroblasts. *PLoS One.* 9:e106554. http://dx.doi.org/10.1371/journal.pone.0106554

Chen, P.I., K. Schauer, C. Kong, A.R. Harding, B. Goud, and P.D. Stahl. 2014b. Rab5 isoforms orchestrate a "division of labor" in the endocytic network; Rab5C modulates Rac-mediated cell motility. *PLoS One.* 9:e90384. http://dx.doi.org/10.1371/journal.pone.0090384

Clark, K., R. Pankov, M.A. Travis, J.A. Askari, A.P. Mould, S.E. Craig, P. Newham, K.M. Yamada, and M.J. Humphries. 2005. A specific $\alpha_5\beta_1$-integrin conformation promotes directional integrin translocation and fibronectin matrix formation. *J. Cell Sci.* 118:291–300. http://dx.doi.org/10.1242/jcs.01623

Clark, K., J.D. Howe, C.E. Pullar, J.A. Green, V.V. Artym, K.M. Yamada, and D.R. Critchley. 2010. Tensin 2 modulates cell contractility in 3D collagen gels through the RhoGAP DLC1. *J. Cell. Biochem.* 109:808–817.

Faubert, B., G. Boily, S. Izreig, T. Griss, B. Samborska, Z. Dong, F. Dupuy, C. Chambers, B.J. Fuerth, B. Viollet, et al. 2013. AMPK is a negative regulator of the Warburg effect and suppresses tumor growth in vivo. *Cell Metab.* 17:113–124. http://dx.doi.org/10.1016/j.cmet.2012.12.001

Geiger, B., and K.M. Yamada. 2011. Molecular architecture and function of matrix adhesions. *Cold Spring Harb. Perspect. Biol.* 3:a005033. http://dx.doi.org/10.1101/cshperspect.a005033

Geiger, B., A. Bershadsky, R. Pankov, and K.M. Yamada. 2001. Transmembrane crosstalk between the extracellular matrix and the cytoskeleton crosstalk. *Nat. Rev. Mol. Cell Biol.* 2:793–805. http://dx.doi.org/10.1038/35099066

Gudzenko, T., and C.M. Franz. 2015. Studying early stages of fibronectin fibrillogenesis in living cells by atomic force microscopy. *Mol. Biol. Cell.* 26:3190–3204. http://dx.doi.org/10.1091/mbc.E14-05-1026

Guet, D., K. Mandal, M. Pinot, J. Hoffmann, Y. Abidine, W. Sigaut, S. Bardin, K. Schauer, B. Goud, and J.B. Manneville. 2014. Mechanical role of actin dynamics in the rheology of the Golgi complex and in Golgi-associated trafficking events. *Curr. Biol.* 24:1700–1711. http://dx.doi.org/10.1016/j.cub.2014.06.048

Hardie, D.G. 2013. AMPK: a target for drugs and natural products with effects on both diabetes and cancer. *Diabetes.* 62:2164–2172. http://dx.doi.org/10.2337/db13-0368

Hardie, D.G., F.A. Ross, and S.A. Hawley. 2012. AMPK: a nutrient and energy sensor that maintains energy homeostasis. *Nat. Rev. Mol. Cell Biol.* 13:251–262. http://dx.doi.org/10.1038/nrm3311

Horton, E.R., A. Byron, J.A. Askari, D.H. Ng, A. Millon-Frémillon, J. Robertson, E.J. Koper, N.R. Paul, S. Warwood, D. Knight, et al. 2015. Definition of a consensus integrin adhesome and its dynamics during adhesion complex assembly and disassembly. *Nat. Cell Biol.* 17:1577–1587. http://dx.doi.org/10.1038/ncb3257

Horton, E.R., P. Astudillo, M.J. Humphries, and J.D. Humphries. 2016. Mechanosensitivity of integrin adhesion complexes: role of the consensus adhesome. *Exp. Cell Res.* 343:7–13. http://dx.doi.org/10.1016/j.yexcr.2015.10.025

Hughes, P.E., B. Oertli, M. Hansen, F.L. Chou, B.M. Willumsen, and M.H. Ginsberg. 2002. Suppression of integrin activation by activated Ras or Raf does not correlate with bulk activation of ERK MAP kinase. *Mol. Biol. Cell.* 13:2256–2265. http://dx.doi.org/10.1091/mbc.01-10-0480

Humphrey, J.D., E.R. Dufresne, and M.A. Schwartz. 2014. Mechanotransduction and extracellular matrix homeostasis. *Nat. Rev. Mol. Cell Biol.* 15:802–812. http://dx.doi.org/10.1038/nrm3896

Hynes, R.O. 2002. Integrins: bidirectional, allosteric signaling machines. *Cell.* 110:673–687. http://dx.doi.org/10.1016/S0092-8674(02)00971-6

Jacquemet, G., D.M. Green, R.E. Bridgewater, A. von Kriegsheim, M.J. Humphries, J.C. Norman, and P.T. Caswell. 2013. RCP-driven α5β1 recycling suppresses Rac and promotes RhoA activity via the RacGAP1-IQGAP1 complex. *J. Cell Biol.* 202:917–935. http://dx.doi.org/10.1083/jcb.201302041

Kim, C., F. Ye, and M.H. Ginsberg. 2011. Regulation of integrin activation. *Annu. Rev. Cell Dev. Biol.* 27:321–345. http://dx.doi.org/10.1146/annurev-cellbio-100109-104104

Lee, J.H., H. Koh, M. Kim, Y. Kim, S.Y. Lee, R.E. Karess, S.H. Lee, M. Shong, J.M. Kim, J. Kim, and J. Chung. 2007. Energy-dependent regulation of cell structure by AMP-activated protein kinase. *Nature.* 447:1017–1020. http://dx.doi.org/10.1038/nature05828

Lemmon, C.A., C.S. Chen, and L.H. Romer. 2009. Cell traction forces direct fibronectin matrix assembly. *Biophys. J.* 96:729–738. http://dx.doi.org/10.1016/j.bpj.2008.10.009

Lemons, J.M., X.J. Feng, B.D. Bennett, A. Legesse-Miller, E.L. Johnson, I. Raitman, E.A. Pollina, H.A. Rabitz, J.D. Rabinowitz, and H.A. Coller. 2010. Quiescent fibroblasts exhibit high metabolic activity. *PLoS Biol.* 8:e1000514. http://dx.doi.org/10.1371/journal.pbio.1000514

Lim, J.Y., M.A. Oh, W.H. Kim, H.Y. Sohn, and S.I. Park. 2012. AMP-activated protein kinase inhibits TGF-β-induced fibrogenic responses of hepatic stellate cells by targeting transcriptional coactivator p300. *J. Cell. Physiol.* 227:1081–1089. http://dx.doi.org/10.1002/jcp.22824

Lin, G.L., D.M. Cohen, R.A. Desai, M.T. Breckenridge, L. Gao, M.J. Humphries, and C.S. Chen. 2013. Activation of beta 1 but not beta 3 integrin increases cell traction forces. *FEBS Lett.* 587:763–769. http://dx.doi.org/10.1016/j.febslet.2013.01.068

Liu, J., W. Liu, H. Ying, W. Zhao, and H. Zhang. 2013. Analysis of microRNA expression profile induced by AICAR in mouse hepatocytes. *Gene.* 512:364–372. http://dx.doi.org/10.1016/j.gene.2012.09.118

Lo, S.H., Q. An, S. Bao, W.K. Wong, Y. Liu, P.A. Janmey, J.H. Hartwig, and L.B. Chen. 1994a. Molecular cloning of chick cardiac muscle tensin. Full-length cDNA sequence, expression, and characterization. *J. Biol. Chem.* 269:22310–22319.

Lo, S.H., P.A. Janmey, J.H. Hartwig, and L.B. Chen. 1994b. Interactions of tensin with actin and identification of its three distinct actin-binding domains. *J. Cell Biol.* 125:1067–1075. http://dx.doi.org/10.1083/jcb.125.5.1067

Mandal, K., A. Asnacios, B. Goud, and J.B. Manneville. 2016. Mapping intracellular mechanics on micropatterned substrates. *Proc. Natl. Acad. Sci. USA.* 113:E7159–E7168. http://dx.doi.org/10.1073/pnas.1605112113

McCleverty, C.J., D.C. Lin, and R.C. Liddington. 2007. Structure of the PTB domain of tensin1 and a model for its recruitment to fibrillar adhesions. *Protein Sci.* 16:1223–1229. https://doi.org/10.1110/ps.072798707

Mihaylova, M.M., and R.J. Shaw. 2011. The AMPK signalling pathway coordinates cell growth, autophagy and metabolism. *Nat. Cell Biol.* 13:1016–1023. http://dx.doi.org/10.1038/ncb2329

Mirouse, V., and M. Billaud. 2011. The LKB1/AMPK polarity pathway. *FEBS Lett.* 585:981–985. http://dx.doi.org/10.1016/j.febslet.2010.12.025

Nakano, A., H. Kato, T. Watanabe, K.D. Min, S. Yamazaki, Y. Asano, O. Seguchi, S. Higo, Y. Shintani, H. Asanuma, et al. 2010. AMPK controls the speed of microtubule polymerization and directional cell migration through CLIP-170 phosphorylation. *Nat. Cell Biol.* 12:583–590. http://dx.doi.org/10.1038/ncb2060

Nevo, J., A. Mai, S. Tuomi, T. Pellinen, O.T. Pentikäinen, P. Heikkilä, J. Lundin, H. Joensuu, P. Bono, and J. Ivaska. 2010. Mammary-derived growth inhibitor (MDGI) interacts with integrin α-subunits and suppresses integrin activity and invasion. *Oncogene.* 29:6452–6463. http://dx.doi.org/10.1038/onc.2010.376

Pankov, R., E. Cukierman, B.Z. Katz, K. Matsumoto, D.C. Lin, S. Lin, C. Hahn, and K.M. Yamada. 2000. Integrin dynamics and matrix assembly: tensin-dependent translocation of $\alpha_5\beta_1$ integrins promotes early fibronectin fibrillogenesis. *J. Cell Biol.* 148:1075–1090. http://dx.doi.org/10.1083/jcb.148.5.1075

Pellinen, T., J.K. Rantala, A. Arjonen, J.P. Mpindi, O. Kallioniemi, and J. Ivaska. 2012. A functional genetic screen reveals new regulators of β1-integrin activity. *J. Cell Sci.* 125:649–661. http://dx.doi.org/10.1242/jcs.090704

Pelouch, V., I.M. Dixon, L. Golfman, R.E. Beamish, and N.S. Dhalla. 1993. Role of extracellular matrix proteins in heart function. *Mol. Cell. Biochem.* 129:101–120. http://dx.doi.org/10.1007/BF00926359

Pylayeva, Y., and F.G. Giancotti. 2007. Tensin relief facilitates migration. *Nat. Cell Biol.* 9:877–879. http://dx.doi.org/10.1038/ncb0807-877

Rainero, E., J.D. Howe, P.T. Caswell, N.B. Jamieson, K. Anderson, D.R. Critchley, L. Machesky, and J.C. Norman. 2015. Ligand-occupied integrin internalization links nutrient signaling to invasive migration. *Cell Reports.* 10:398–413.

Rantala, J.K., J. Pouwels, T. Pellinen, S. Veltel, P. Laasola, E. Mattila, C.S. Potter, T. Duffy, J.P. Sundberg, O. Kallioniemi, et al. 2011. SHARPIN is an endogenous inhibitor of β1-integrin activation. *Nat. Cell Biol.* 13:1315–1324. http://dx.doi.org/10.1038/ncb2340

Robertson, J., G. Jacquemet, A. Byron, M.C. Jones, S. Warwood, J.N. Selley, D. Knight, J.D. Humphries, and M.J. Humphries. 2015. Defining the phospho-adhesome through the phosphoproteomic analysis of integrin signalling. *Nat. Commun.* 6:6265. http://dx.doi.org/10.1038/ncomms7265

Satriano, J., K. Sharma, R.C. Blantz, and A. Deng. 2013. Induction of AMPK activity corrects early pathophysiological alterations in the subtotal nephrectomy model of chronic kidney disease. *Am. J. Physiol. Renal Physiol.* 305:F727–F733. http://dx.doi.org/10.1152/ajprenal.00293.2013

Schaffer, B.E., R.S. Levin, N.T. Hertz, T.J. Maures, M.L. Schoof, P.E. Hollstein, B.A. Benayoun, M.R. Banko, R.J. Shaw, K.M. Shokat, and A. Brunet. 2015. Identification of AMPK phosphorylation sites reveals a network of proteins involved in cell invasion and facilitates large-scale substrate prediction. *Cell Metab.* 22:907–921. http://dx.doi.org/10.1016/j.cmet.2015.09.009

Schiller, H.B., M.R. Hermann, J. Polleux, T. Vignaud, S. Zanivan, C.C. Friedel, Z. Sun, A. Raducanu, K.E. Gottschalk, M. Théry, et al. 2013. β_1- and α_v-class integrins cooperate to regulate myosin II during rigidity sensing of fibronectin-based microenvironments. *Nat. Cell Biol.* 15:625–636. http://dx.doi.org/10.1038/ncb2747

Schindelin, J., I. Arganda-Carreras, E. Frise, V. Kaynig, M. Longair, T. Pietzsch, S. Preibisch, C. Rueden, S. Saalfeld, B. Schmid, et al. 2012. Fiji: an open-source platform for biological-image analysis. *Nat. Methods.* 9:676–682. http://dx.doi.org/10.1038/nmeth.2019

Schwarz, U.S., and M.L. Gardel. 2012. United we stand: integrating the actin cytoskeleton and cell-matrix adhesions in cellular mechanotransduction. *J. Cell Sci.* 125:3051–3060. http://dx.doi.org/10.1242/jcs.093716

Suh, E.J., M.Y. Remillard, A. Legesse-Miller, E.L. Johnson, J.M. Lemons, T.R. Chapman, J.J. Forman, M. Kojima, E.S. Silberman, and H.A. Coller. 2012. A microRNA network regulates proliferative timing and extracellular matrix synthesis during cellular quiescence in fibroblasts. *Genome Biol.* 13:R121. http://dx.doi.org/10.1186/gb-2012-13-12-r121

Tadokoro, S., S.J. Shattil, K. Eto, V. Tai, R.C. Liddington, J.M. de Pereda, M.H. Ginsberg, and D.A. Calderwood. 2003. Talin binding to integrin β tails: a final common step in integrin activation. *Science.* 302:103–106. http://dx.doi.org/10.1126/science.1086652

Theodosiou, M., M. Widmaier, R.T. Böttcher, E. Rognoni, M. Veelders, M. Bharadwaj, A. Lambacher, K. Austen, D.J. Müller, R. Zent, and R. Fässler. 2016. Kindlin-2 cooperates with talin to activate integrins and induces cell spreading by directly binding paxillin. *eLife.* 5:e10130. http://dx.doi.org/10.7554/eLife.10130

Wang, S., C. Zhang, M. Zhang, B. Liang, H. Zhu, J. Lee, B. Viollet, L. Xia, Y. Zhang, and M.H. Zou. 2012. Activation of AMP-activated protein kinase α2 by nicotine instigates formation of abdominal aortic aneurysms in mice *in vivo*. *Nat. Med.* 18:902–910. http://dx.doi.org/10.1038/nm.2711

Yan, Y., S. Ollila, I.P. Wong, T. Vallenius, J.J. Palvimo, K. Vaahtomeri, and T.P. Mäkelä. 2015. SUMOylation of AMPKα1 by PIAS4 specifically regulates mTORC1 signalling. *Nat. Commun.* 6:8979. http://dx.doi.org/10.1038/ncomms9979

Zamir, E., M. Katz, Y. Posen, N. Erez, K.M. Yamada, B.Z. Katz, S. Lin, D.C. Lin, A. Bershadsky, Z. Kam, and B. Geiger. 2000. Dynamics and segregation of cell-matrix adhesions in cultured fibroblasts. *Nat. Cell Biol.* 2:191–196.

Zhang, L., J. Li, L.H. Young, and M.J. Caplan. 2006. AMP-activated protein kinase regulates the assembly of epithelial tight junctions. *Proc. Natl. Acad. Sci. USA.* 103:17272–17277. http://dx.doi.org/10.1073/pnas.0608531103